Hydroxylpyromorphite, a mineral important to lead remediation: Modern description and characterization

TRAVIS A. OLDS^{1,*}, ANTHONY R. KAMPF^{2,†}, JOHN F. RAKOVAN³, PETER C. BURNS^{4,5,‡}, OWEN P. MILLS⁶, AND CULLEN LAUGHLIN-YURS⁷

¹Section of Minerals and Earth Sciences, Carnegie Museum of Natural History, 4400 Forbes Avenue, Pittsburgh, Pennsylvania 15213, U.S.A.

²Mineral Sciences Department, Natural History Museum of Los Angeles County, 900 Exposition Boulevard, Los Angeles, California 90007, U.S.A.

³Department of Geology and Environmental Earth Science, Miami University, Oxford, Ohio 45056, U.S.A.

⁴Department of Civil and Environmental Engineering and Earth Sciences, University of Notre Dame, Notre Dame, Indiana 46556, U.S.A.

⁵Department of Chemistry and Biochemistry, University of Notre Dame, Notre Dame, Indiana 46556, U.S.A.

⁶Applied Chemical and Morphological Analysis Laboratory, Michigan Technological University, Houghton, Michigan 49931, U.S.A.

⁷513 Iron Street, Norway, Michigan 49870, U.S.A.

ABSTRACT

Hydroxylpyromorphite, Pb₅(PO₄)₃(OH), has been documented in the literature as a synthetic and naturally occurring phase for some time but has not previously been formally described as a mineral. It is fully described here for the first time using crystals collected underground in the Copps mine, Gogebic County, Michigan. Hydroxylpyromorphite occurs as aggregates of randomly oriented hexagonal prisms, primarily between about 20–35 μm in length and 6–10 μm in diameter. The mineral is colorless and translucent with vitreous luster and white streak. The Mohs hardness is ~3½-4; the tenacity is brittle, the fracture is irregular, and indistinct cleavage was observed on {001}. Electron microprobe analyses provided the empirical formula Pb_{4.97}(PO₄)₃(OH_{0.69}F_{0.33}Cl_{0.06})_{Σ1.08}. The calculated density using the measured composition is 7.32 g/cm³. Powder X-ray diffraction data for the type material is compared to data previously reported for hydroxylpyromorphite from the talc mine at Rabenwald, Austria, and from Whytes Cleuch, Wanlockhead, Scotland. Hydroxylpyromorphite is hexagonal, P63/m, at 100 K, a = 9.7872(14), c = 7.3070(10) Å, V = 606.16(19) Å³, and Z = 2. The structure $[R_1 = 0.0181]$ for 494 $F>4\sigma(F)$ reflections] reveals that hydroxylpyromorphite adopts a column anion arrangement distinct from other members of the apatite supergroup due to the presence of fluorine and steric constraints imposed by stereoactive lone-pair electrons of Pb2+ cations. The F- anion sites are displaced slightly from hydroxyl oxygen anions, which allows for stronger hydrogen-bonding interactions that may in turn stabilize the observed column-anion arrangement and overall structure. Our modern characterization of hydroxylpyromorphite provides deeper understanding to a mineral useful for remediation of lead-contaminated water.

Keywords: Hydroxylpyromorphite, apatite, crystal structure, Copps mine, infrared spectroscopy, Michigan, anion column

Introduction

The apatite supergroup comprises a series of structurally related minerals with the general formula $^{IX}M1_2^{VII}M2_3(^{IV}TO_4)_3X$ based upon a heteropolyhedral framework of metallic (M = Ca^{2+} , Pb^{2+} , Cd^{2+} , Ba^{2+} , Sr^{2+} , Mn^{2+} , Na^+ , Ce^{3+} , La^{3+} , Y^{3+} , Bi^{3+}) and tetrahedral cations (T = P^{5+} , V^{5+} , As^{5+} , Si^{4+} , S^{6+} , B^{3+}) with columns containing the X anions: F^- , (OH) $^-$, or Cl $^-$ (Pasero et al. 2010). More than fifty years of crystallographic studies of mineralogical, biological and synthetic apatite phases have revealed that extensive anion solid solution occurs among the group members and that certain species exhibit specific anion-column ordering schemes dependent on size, site occupancy, and the chemical makeup of the anion column (Hughes and Rakovan 2015; White

and ZhiLi 2003). Our understanding of anion-column ordering in the calcium phosphate apatites is now rather well-established based on several studies of natural and synthetic samples (Hughes et al. 2014, 2016, 2018; Kelly et al. 2017). However, details of anion ordering in the pyromorphite group are incomplete due to missing data for the fluor and hydroxyl members.

In the existing literature, numerous references have been made to "hydroxypyromorphite, hydroxopyromorphite, lead apatite, or lead hydroxyapatite" compounds as both synthetic and natural material, although until now the crystal structure of hydroxylpyromorphite found in Nature was not determined, nor formally considered a mineral (Brückner et al. 1995; Cockbain 1968; Lower et al. 1998; Mavropoulos et al. 2002; Zhu et al. 2016). Here for the first time, we provide a full structural analysis of the mineral hydroxylpyromorphite.

The mineral and its name have been approved by the Commission on New Minerals, Nomenclature and Classification of

^{*} E-mail: oldst@carnegiemnh.org. Orcid 0000-0001-5333-0802

[†] Orcid 0000-0001-8084-2563

[‡] Orcid 0000-0002-2319-9628

the International Mineralogical Association (IMA2017-075). The prefix "hydroxyl" is used in accordance with the nomenclature scheme for the apatite supergroup (Hatert et al. 2013; Pasero et al. 2010). The description is based on one holotype specimen deposited in the collections of the Natural History Museum of Los Angeles County, California, U.S.A., catalog number 66627.

OCCURRENCE

Hydroxylpyromorphite crystals were collected by Shawn M. Carlson and one of the authors (C.L.) in 2015 at the Copps mine, Gogebic County, Michigan. This "mine" is actually a late 19th century test exploration consisting of approximately eleven small adits, pits, trenches, and shafts spanning a distance of about 225 m, and located in sections 14, 15, and 22, T47N, R43W (Carlson et al. 2017). The exploration tested discontinuous and sub-economic precious and base-metal mineralization, mainly Pb, Cu, and Ag contained within the Early Proterozoic Copps Formation (Baraga Group of the Marquette Range Supergroup), a formation comprised primarily of metagraywacke and conglomeratic, ferruginous quartzite (Klasner et al. 1998). Hydroxylpyromorphite has so far been identified from a single specimen of vein quartz and its only intimate association is with quartz as vug linings, but more generally is associated with twenty-one minerals, one mineraloid, and seven unknowns that have been documented at the prospect. The identified minerals include anglesite, beaverite-(Cu), calcite, cerussite, chalcopyrite, chamosite, corkite, covellite, dolomite, galena, goethite, gypsum, hematite, jarosite, "K-feldspar," malachite, plumbojarosite, pyrite, quartz, "sericite," and sphalerite (Carlson et al. 2017). The morphology and association of hydroxylpyromorphite suggest that it is a geogenic secondary Pb phase and is not post-mining in origin.

In what may be the first report of natural hydroxylpyromorphite, Temple (1956) identified a lead phosphate mineral from an unspecified vein at Whytes Cleuch, Wanlockhead, Dumfries and Galloway, Scotland, U.K., which he described as "lead hydroxyapatite," but provided no chemical data. In the words of Temple (1956), "The mineral appears to represent a further substitution in the pyromorphite group, the hydroxyl group substituting for chloride." It forms powdery white coatings associated with polysphaerite [phosphohedyphane, Ca₂Pb₃(PO₄)₃Cl], as pseudomorphs after galena. We have sought and tested similar material from Whytes Cleuch; however, in the single specimen studied, we have only identified phosphohedyphane and anglesite. Single crystals of hydroxylpyromorphite, if present, were too intimately admixed with phosphohedyphane and far too small for conventional singlecrystal X-ray diffraction (SCXRD) analysis. This was likewise the case for material from a third reported occurrence of thin white coatings of finely crystalline hydroxylpyromorphite from the talc mine at Rabenwald, Anger, Weiz, Styria, Austria (Kolitsch and Lóránth 2016). According to the website Mindat.org (accessed July 2020), several other reported hydroxylpyromorphite occurrences exist, but we have not been able to confirm their validity. Two samples tested from the Motel 22 occurrence, Brady Township, Huntingdon Co., Pennsylvania, U.S.A., were found to contain only anglesite and cerussite. An additional occurrence of anthropogenic "hydroxylpyromorphite" is reported by Kirchner along with other secondary Pb, Cu, and As minerals on medieval slag heaps south of Radhausberg, Austria (Kirchner et al. 2007).

Our difficulty locating suitable material for single-crystal structure determination may attest to why the mineral has remained undescribed until now; however, we are able to provide a comparison of X-ray powder diffraction data for Copps mine crystals to the original "lead hydroxyapatite" data given by Temple (1956), and hydroxylpyromorphite from Kolitsch and Lóránth (2016). While we acknowledge that the Copps mine is not the first reported occurrence for hydroxylpyromorphite, it is the first to provide suitable material for a full description of the phase.

PHYSICAL AND OPTICAL PROPERTIES

On the holotype specimen, hydroxylpyromorphite crystals are arranged in aggregates of randomly oriented colorless hexagonal prisms, primarily between about 20–35 μ m in length and 6–10 μ m in diameter (Fig. 1), although several highly elongated crystals reaching 250 μ m in length were also found. Crystals exhibit the {100} prism and are terminated by the {101} pyramid (Fig. 2). They are translucent with a vitreous luster, have a white streak and are non-fluorescent under both long- and short-wave ultraviolet illumination. The crystals are brittle with indistinct {001} cleavage

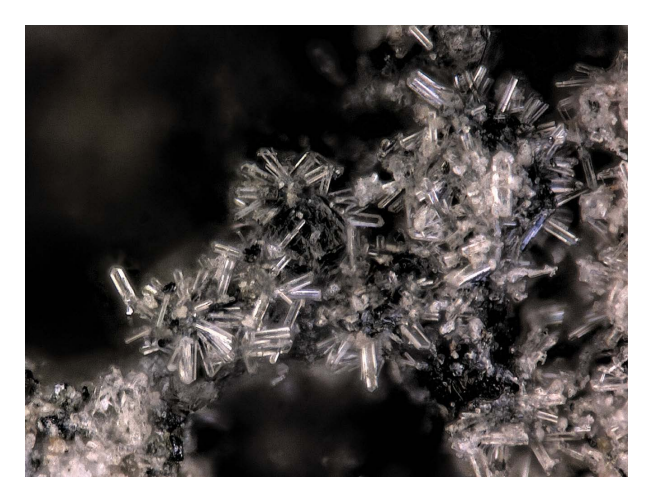


FIGURE 1. Aggregates of prismatic hydroxylpyromorphite crystals on quartz. Horizontal field of view is 0.45 mm. (Color online.)

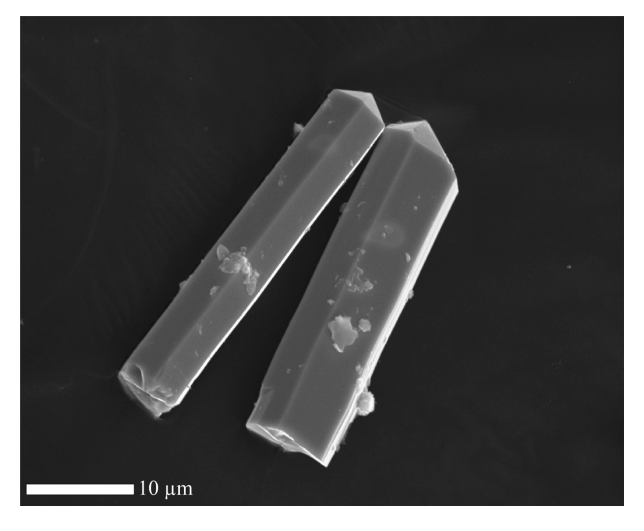


FIGURE 2. SEM image of hydroxylpyromorphite crystals.

and irregular fracture. The Mohs hardness is about 3.5–4 based on scratch tests. The density could not be measured due to the limited availability of material and because it exceeds that of available heavy liquids. The calculated density is 7.32 g/cm⁻³ based on the empirical formula and 7.33 g/cm³ for the ideal formula.

Optically, hydroxylpyromorphite is uniaxial (–), with $\omega-\epsilon$ birefringence = 0.03. The small crystal size and high indices of refraction made the measurement of indices of refraction impractical. The predicted average index of refraction based upon the Gladstone-Dale relationship is 2.04. The indices of refraction of pyromorphite are slightly higher by comparison, $\omega=2.058, \epsilon=2.048$ (Anthony et al. 2000).

INFRARED SPECTROSCOPY

Attenuated total reflectance (ATR) Fourier-transform infrared (FTIR) spectra were obtained using a liquid N2-cooled SENSIR Technologies IlluminatIR mounted to an Olympus BX51 microscope. A ContactIR ATR objective (diamond and ZnSe lens) was pressed into crystals of hydroxylpyromorphite and spectra were collected from 4000 to 650 cm⁻¹. The infrared spectrum is shown in Figure 3. Broad hydroxyl stretching vibrations occur between ~3600 and 3000 cm⁻¹. Approximate O-H···O hydrogen bondlengths calculated from the observed stretching frequencies lie within the range \sim 3.2 to 2.7 Å using the correlation function given by Libowitzky (1999). Hydrogen-bonding interactions in the crystal structure are weak (≥ 3 Å), and thus stronger H-bonding interactions observed in the IR spectrum may be attributable to adsorbed H₂O (Ishikawa et al. 1989). A broad and weak band centered near ~1950 cm⁻¹ is likely a combination band (v₃ PO₄ + v_1 PO₄). The v_3 anti-symmetric stretching mode of PO₄ units occurs as moderately strong bands at 1053 and 1000 cm⁻¹. The ν₁ PO₄ symmetric stretching mode is found as a very strong band at 917 cm⁻¹, and the weak v₄ bending mode of PO₄ occurs at 764 cm⁻¹.

CHEMICAL COMPOSITION

Chemical analyses (12) were performed using a JEOL JXA-773 electron microprobe operating at an accelerating voltage of 15 kV, with a beam current of 10 nA and 10 μ m spot diameter. Crystals were oriented and analyzed using surfaces perpendicular to the c axis (see below). Hydroxylpyromorphite contains major Pb, P, and O, with minor F and trace Cl. No other elements were detected. Matrix effects were accounted for using the ZAF correction routine (Armstrong 1988). Due to the limited amount of material available, the H₂O content was not measured and is instead calculated by stoichiometry with respect to the structure. Analytical data are given in Table 1. The empirical formula, calculated on the basis of 3 P atoms per formula unit (apfu) is Pb_{4.97}(PO₄)₃(OH_{0.69}F_{0.33}Cl_{0.06})_{21.08}. The ideal formula is Pb₅(PO₄)₃(OH), which requires PbO 83.41, P₂O₅ 15.91, H₂O 0.67, total 100 wt%.

Electron-beam-induced halogen migration is commonly observed in fluorapatites and chlorapatites (Stock et al. 2015), where an inaccurate measured halogen concentration is caused by accumulation of those elements near the analysis surface. Migration is most pronounced when the electron beam impinges on (001) sections, parallel to the anion columns in the apatite structure, whereas minimal migration occurs in {100} sections, that is, when the beam is normal to the **c** axis (Stormer et al.

1993). After prolonged exposure to the electron beam, a decrease of measured signals attributed to F and Cl corresponds to loss due to volatility. We conducted a series of microprobe experiments using hydroxylpyromorphite crystals with their ${\bf c}$ axis oriented parallel to the beam to monitor anion migration. Raw counts for F in hydroxylpyromorphite were collected using sequential 5 s count times up to 2 min at 15 kV, 25 nA, and 1 μ m beam diameter. No statistically significant change in the F signal over the period of two minutes was observed, suggesting that significant electronbeam induced F migration does not occur, at least on this time scale (Online Material¹ Fig. OM1). The very small size of the polished crystal sections (~5 μ m) and low total F and Cl content may also lead to poor resolution of halogen migration here.

An additional single spot analysis was noted to display anomalously high F content, 1.02 wt%, corresponding to the empirical formula Pb_{5.23}(PO₄)₃(F_{0.76}OH_{0.21}Cl_{0.08})_{Σ1.04}. This single analysis may correspond to the yet undescribed F-analog of pyromorphite, "fluorpyromorphite," but was considered to be of low quality due to the high proportion of Pb:P. Subsequent analyses have not revealed demonstrably F-dominant crystals, nor have we observed any clear zonation of F content within the resolution of the microprobe that might suggest the F-dominant analog exists at the Copps mine.

POWDER X-RAY DIFFRACTION

X-ray powder diffraction data were obtained using a Rigaku R-Axis Rapid II curved imaging plate microdiffractometer with monochromatized Mo $K\alpha$ radiation. A Gandolfi-like motion on the ϕ and ω axes was used to randomize diffraction from the

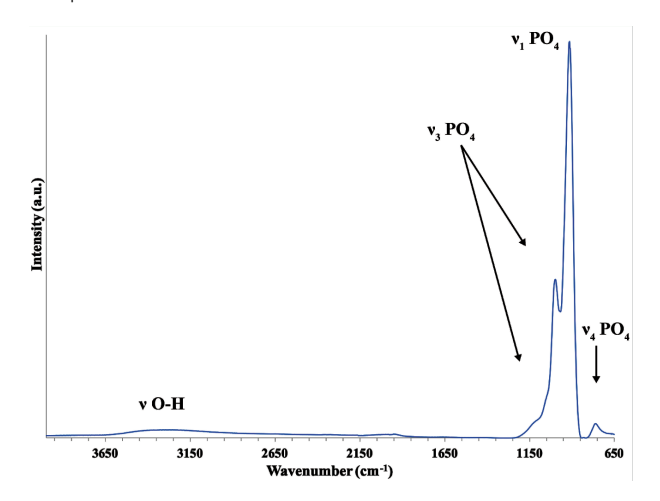


FIGURE 3. The infrared spectrum of hydroxylpyromorphite from 4000 to 650 cm⁻¹. (Color online.)

TABLE 1. Chemical composition (in wt%) for hydroxylpyromorphite

Constituent	uent Mean Rang		St. dev.	Standard
PbO	82.20	80.21-83.63	1.19	galena
P_2O_5	15.77	14.54-16.33	0.67	fluorapatite
CI	0.15	0.10-0.28	0.05	tugtupite
F	0.46	0.23-0.69	0.21	LiF
H_2O^a	0.46			
O=CI	-0.03			
O=F	-0.19			
Total	98.82			

^a Based on the structure.

sample. Observed *d*-values and intensities were derived by profile fitting using JADE 2010 software (Materials Data, Inc.). Data (in angstroms for Mo $K\alpha$) are given in Online Material¹ Table OM1. Unit-cell parameters refined from the powder data using JADE 2010 with whole pattern fitting in space group $P6_3/m$ are: a = 9.7858(14) Å, c = 7.3072(11) Å, $V = 606.0(2) \text{ Å}^3$.

The powder X-ray diffraction data for Copps mine hydroxylpyromorphite presented here agrees favorably with the lines observed by Temple (1956) for "lead hydroxyapatite" from Whytes Cleuch and synthetic material listed by Hey (1950), as well as with data measured for hydroxylpyromorphite from the talc mine at Rabenwald, Austria (Uwe Kolitsch, personal communication; Table 2).

SINGLE-CRYSTAL X-RAY DIFFRACTION

A small elongated hexagonal prism was chosen for the singlecrystal X-ray diffraction experiment. Data were collected at 100 K using monochromatized MoKα X-rays from a microfocus source and an Apex II CCD-based detector mounted onto a Bruker Apex II Quazar three-circle diffractometer. Reflections were integrated and corrected for Lorentz, polarization, and background effects using the Bruker program SAINT. A multi-scan semi-empirical absorption correction was applied using equivalent reflections in SADABS-2012 (Krause et al. 2015). An initial structure model was obtained using SHELXT (Sheldrick 2015a) in space group $P6_3/m$, and refinements were made by full-matrix least-squares on F2 using SHELXL-2016 (Sheldrick 2015b). All atoms except those in the anion column were refined with anisotropic displacement parameters, and the U_{eq} of atom H1 set to 1.2 times that of its donor O atom, O4. Data collection and refinement information are presented in the Online Material¹ Tables OM2-OM5. A CIF¹ file for the structure of hydroxylpyromorphite is available.

FEATURES OF THE CRYSTAL STRUCTURE

The crystal structure is a heteropolyhedral framework consisting of PbO₉ and PbO₆(OH)₂ polyhedra and phosphate (PO₄) tetrahedra arranged into the well-known apatite-type structure (Fig. 4). Hexamers of Pb2-centered polyhedra share a central atom O4 located on (0,0,0), the oxygen atom of the hydroxyl anion, forming columnar units that extend along [001]. A second structural unit built from Pb1-centered polyhedra consists of simple chains that extend along [001] and connect three sets of

TABLE 2. Comparison of powder diffraction data, I, and d (Å) for hydroxylpyromorphite of different origins

			_					
	tes Cleuch	Raber	nwalda	Syn	thetic	Co	pp	s mine
(Tem	nple 1956)			(Hey	1950)	(T	his	work)
fs	4.06	fs	4.05	24	4.03	18	3	4.08
vw	3.56	w	3.56	16	3.61	6		3.67
vw	3.18	wb	3.23	16	3.18	21		3.21
VS	2.92	VS	2.90	100	2.91	10	0	2.93
VW	2.82	vwb	2.37	8	2.82	13	3	2.82
W	2.02	vw	2.02	16	2.02	21		2.04
vw	1.96	vw	1.97	8	1.96	9		1.98
W	1.91	vw	1.93	16	1.91	23	3	1.94
VW	1.88	w	1.88	8	1.86	15	5	1.85
VW	1.82	wb	1.83	16	1.82	24	ŀ	1.83
VW	1.56	vwbb	1.59	8	1.57	17	7	1.59
vw	1.51	vwbb	1.50	16	1.51	10)	1.49

Notes: s = strong, vs = very strong, vw = very weak, vs = very broad. We Kolitsch (personal communication, May 2018). Data obtained using a KappaCCD single-crystal diffractometer, Gandolfi-like digital powder pattern, MoKa, crystal-detector distance 38 mm.

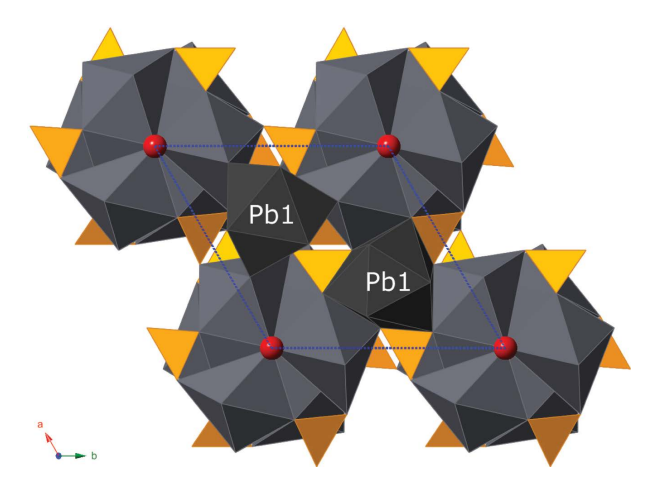


FIGURE 4. The structure of hydroxylpyromorphite as viewed down the **c** axis. Lead (shades of gray), phosphorus (orange), oxygen of hydroxyl molecules (red). (Color online.)

hexamers such that six chains adorn each column of hexamers. Phosphate tetrahedra decorate the chains and columns that connect the Pb polyhedra as well as the hexamer columns to chains.

The P atom position in hydroxylpyromorphite is coordinated by four oxygen atoms in a tetrahedral arrangement, and the average P-O bond distance is 1.544 Å with little variance (Online Material¹ Table OM4). The coordination environment of atom Pb1 takes the shape of a tricapped trigonal prism by bonding to nine phosphate O atoms with an average bond distance of 2.703 Å. Three of the nine bonds to Pb1 are short with O2 at 2.512 Å, with three additional long bonds to O1 at 2.724 Å, and three to O3 at 2.873 Å. The large bond length variance and cis coordination of the short Pb1-O bonds indicate a stereochemically active 6s² lone pair of electrons, which due to symmetry constraints, necessitates their placement along the threefold rotation axis between pairs of Pb1 atoms and directed toward the pyramidal void space formed by O1 or O2 atoms (Dai et al. 1991). The lone pair may reside predominantly in the larger void formed by O1 atoms, with a void volume measuring ~30 Å³, rather than that formed by O2 atoms, with a slightly smaller ~23 Å³ void. Furthermore, at 3.694(1) Å, the Pb1-Pb1 distance through the O1 triangle is ~0.08 Å longer than the Pb1-Pb1 distance through the O2 triangle, supporting dominant occupancy of the lone pair within the O1 void.

Atom Pb2 forms six bonds with O atoms of phosphate groups and two hydroxyl oxygen atoms (O4) in the column, giving an eightfold-coordinated irregular polyhedron with a <Pb2-O> bond distance of 2.707 Å. These bonds also exhibit variable length with lopsided long and short bonds provoked by $6s^2$ lone-pair electrons and include a short 2.398 Å bond to O1 and four relatively short bonds to O3, with two at 2.595 Å and two at 2.637 Å. The long bond to O2 at 2.930 Å and two long bonds with O4 at 2.932 Å accommodate space for the lone-pair electrons. Based on symmetry constraints, the Pb2 lone-pair electrons are directed inward and adjacent to the column anions along the $z = \frac{1}{4}$ mirror plane. Their placement imposes several restrictions on the anion column arrangement in hydroxylpyromorphite.

The anisotropic displacement parameters of atom Pb1 are

essentially isotropic in shape; however, atom Pb2 exhibits a threefold greater elongation along the c axis/ U^{33} vector (0.035 Ų) relative to Pb1 (0.012 Ų). The apparent positional disorder is not significant enough to consider splitting of the Pb1 position, though could suggest a long-range averaged displacement due to inhomogeneous column anion arrangements. We cannot, however, discount that the effect may be due to an inadequate absorption correction.

ANION COLUMN ORDERING

The chemical analyses indicate that hydroxylpyromorphite from the Copps mine contains appreciable fluoride (0.33 apfu), and this raises a question regarding its position among OH groups in the anion column. The hydroxyl oxygen atom O4 exhibited signs of site splitting, and a weak Fourier difference density peak $(\sim 1 \text{ e/A}^3)$ was located approximately $\sim 0.7 \text{ Å}$ from O4. Site scattering refinement trials attempted with full H atom occupancy at this peak led to anomalously high displacement parameters and excessive occupancy (>1) of H, as expected for the occupation of a heavier atom, and we proceeded with the refinement of this peak as a partially occupied F atom. Attempts to refine the disorder as a mixed occupancy site containing both F and H were unsuccessful, so the calculated site-scattering from the chemical analyses for F and H, 3.66 epfu, was initially used to guide the disorder refinement with a split-site model containing separate F and H atom sites. In the final iterations, their occupancies and positions were allowed to refine freely.

Overlap of the column anions and steric limitations imposed by Pb2 lone-pair electrons necessitates specific anion-occupancy considerations based on symmetry constraints, resulting in several possible local configurations of anions (Fig. 5). Related through hexagonal symmetry, the F- anions in hydroxylpyromorphite may substitute locally at column anion sites allowing for reversal of the hydrogen-bonding sequence (Fig. 5b). In this case, F occupancy (which requires local O4 vacancy) results in stronger hydrogen-bonding interactions within the column with a F-O distance of 3.02 Å. Hydrogen-bonding interactions in endmember hydroxylpyromorphite are otherwise nonexistent, with O4-O4 donor-acceptor distances measuring >3.6 Å. Thus, unique F sites displaced slightly from O sites in hydroxylpyromorphite may provide for a more stable anion column arrangement through stronger hydrogen-bonding interactions, potentially yielding a more stable structure with respect to end-member fluor- or hydroxylpyromorphite.

Anion column ordering in fluor-, chlor-, and hydroxylapatites has been investigated in depth by others (Hughes et al. 1989, 2014, 2016, 2018; Kelly et al. 2017), and these studies have provided detailed ordering schemes based on steric limitations of the column and anion constituents. In apatite containing roughly equivalent amounts of F and OH, distinct F and OH sites are found, and their ionic radii [F 1.30 Å and O 1.31 Å (Shannon and Prewitt 1969)] permit each site to be occupied simultaneously, with occupancy and ordering considerations. As a result, complete solid solution between binary F-OH apatite exists with end-member defining F and OH sites while maintaining $P6_3/m$ symmetry (Hughes et al. 1989). However, the presence of minor Cl in fluor- and hydroxylapatite can lead to splitting of the Ca2 site to accommodate the large Cl anions

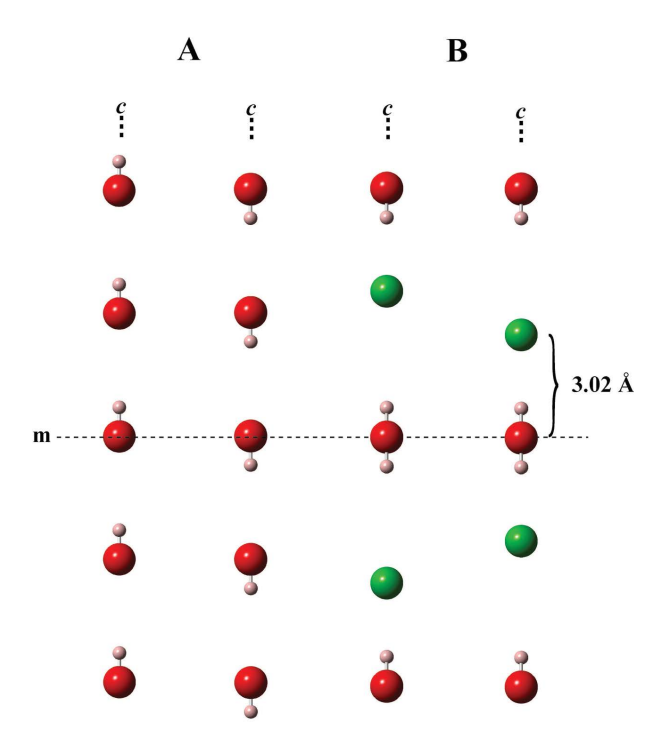


FIGURE 5. Hypothetical local configurations of the anion column for (a) end-member hydroxylpyromorphite and (b) hydroxylpyromorphite containing fluoride. (Color online.)

(Sudarsanan and Young 1978). No such Pb2-site splitting is observed in hydroxylpyromorphite, where the Pb-F bond distance measures 2.58(4) Å, considerably shorter but more ideal than those found in synthetic lead-fluorapatite and Sr-substituted lead-fluorapatite, where Pb/Sr-F bond distances range from ~2.75 to 2.95 Å (Badraoui et al. 2006; Fleet et al. 2010). The Pb-F bond distance in fluorphosphohedyphane is 2.87 Å (Kampf and Housley 2011). Bond-valence analysis of hydroxylpyromorphite indicates that the refined configuration provides ideal sums for all constituents except F at 0.75 v.u., not accounting for partial occupancy or hydrogen bonding [~0.17 v.u.] (Online Material¹ Table OM5). This is more favorable than sums incident to F in fluorphosphohedyphane, 0.594 v.u., and synthetic Pb₅(PO₄)₃F, 0.593 v.u. (Kampf and Housley 2011).

Hughes et al. (2014, 2016, 2018) and Kelly et al. (2017) found the use of isotropic displacement parameters necessary to describe the anion column positions in tertiary and binary hydroxyl-, fluor-, and chlorapatites. This is an effect of the significant anion disorder and Ca site splitting observed in fluor- and hydroxylapatite crystals containing Cl, which due to steric constraints, require introduction of split Cl sites and mixed occupancy O-Cl sites (Fig. 6). We observe similar O-Cl site mixing in hydroxylapyromorphite due to the steric limitations of lone-pair electrons and the formation of an otherwise unfavorably short Pb-Cl bond at \sim 2.58 Å. Thus, at least two column-anion sites are found in hydroxylapyromorphite; including an O/Cl site at z = 0 and a F site at z = 0.087. Such positioning is comparable to the Cl sites found in chlorapatite, mimetite, pyromorphite, alforsite, pieczkaite, and turneaureite, that sit on analogous 2b Wyckoff positions (0,0,0).

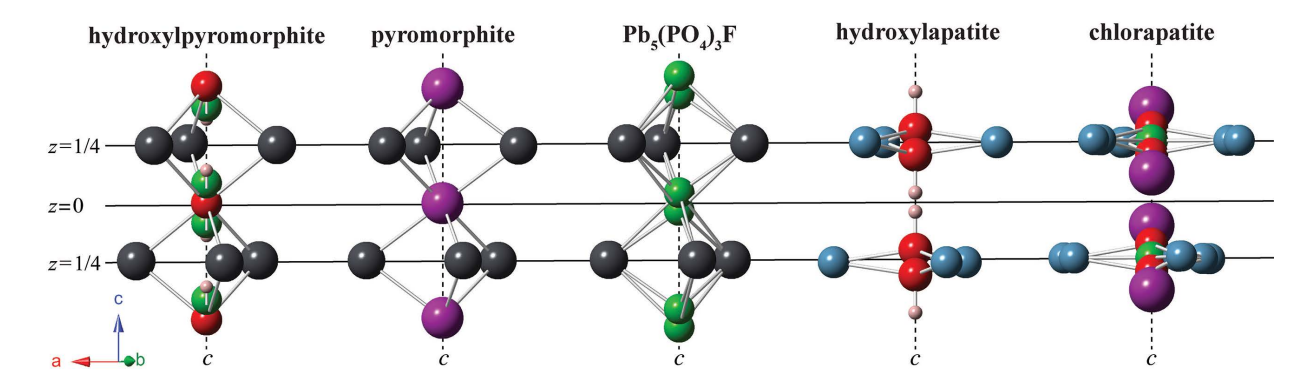


FIGURE 6. A comparison of column anion arrangements in pyromorphite and other apatite group minerals. Hydroxylpyromorphite (this work), pyromorphite (Dai and Hughes 1989), Pb₅(PO₄)₃F (Fleet et al. 2010), hydroxylapatite (Hughes et al. 1989), chlorapatite (Kelly et al. 2017). Lead (dark gray), fluorine (green), oxygen (red), calcium (light blue), chlorine (magenta), and hydrogen (pink). (Color online.)

RELATION TO SYNTHETIC PHASES

Synthetic hydroxylpyromorphite was prepared by Barinova et al. (1998) using hydrothermal methods (260 °C, 100 atm), and its measured single-crystal unit cell parameters are nearly identical to those of crystals from the Copps mine (Table 3). Notable structural differences include slightly larger separation between Pb2-Pb2 pairs and longer Pb2-OH bond distances in natural hydroxylpyromorphite, which is likely a response of lone-pair electrons to the presence of minor F and trace Cl that is absent in the synthetic crystals. Barinova et al. (1998) refined the O of the hydroxyl group at the 2b Wyckoff position (z = 0), in agreement with our description. In contrast, the O of the hydroxyl in the structure refined by Brückner et al. (1995) from powder X-ray diffraction data is displaced slightly from the origin, at z = 0.04. Their model was refined based on starting coordinates from a lead-substituted hydroxylapatite with ~80% Pb content, determined by Bigi et al. (1989). The refinements show clearly that the O atom site of the hydroxyl anion is strongly correlated with Pb content and that with increasing Pb substitution, the O site moves further from the mirror plane and Pb/Ca triangle, shifting closer to z = 0. This suggests that a solid-solution series may extend between hydroxylpyromorphite and the yet undescribed mineral "hydroxylphosphohedyphane" Ca₂Pb₃(PO₄)₃(OH).

In the structure of synthetic fluorpyromorphite, Belokoneva et al. (1982) found that F^- anions assumed a position at z = 0.25, in plane with the triangle of Pb atoms, forming a very short bond with Pb2 of 2.33 Å (1.52 v.u.). In the neutron powder diffraction study by Kim et al. (1997), F atoms sit at z = 0.5/0. It was later shown by Badraoui et al. (2006) using X-ray Rietveld refinement

and by Fleet et al. (2010) using single-crystal X-ray diffraction that the F site adopts a split-atom position at z = 0.449 and 0.461, with 50/50 occupancy. This is in agreement with our findings for hydroxylpyromorphite, where F anions are displaced slightly from O atoms of hydroxyl anions.

White and ZhiLi (2003) examined the influence of stereoactive lone-pair electrons on symmetry and metaprism twist angles in apatites and related structures. Likewise, Baikie et al. (2014) compile both new and old structure data for several natural leadcontaining apatites as a function of temperature, revealing that the twist angle of opposing triangular faces of the framework Pb1O₆ metaprism projected on (001) is sensitive to the anion and tetrahedral cation content. These studies show that metaprism twist angle is inversely related to the cross section of the anionic column and the average effective ionic radius and that the twist angle contracts significantly at lower temperatures. Metaprism twist angles of selected synthetic hydroxyl- and fluorpyromorphites are compared in Table 3. The Pb1 metaprism twist in hydroxylpyromorphite is the smallest angle of those calculated using the method of White and ZhiLi (2003), likely due to the low temperature used for data collection. However, considering the large range of twist angles observed for synthetic hydroxyl- and fluorpyromorphites, it may be interesting to test the influence of variable OH-, F-, Pb, and Ca content on anion ordering and metaprism twist angle.

Because of their essentially identical X-ray scattering factors, it is possible that the refined O and F column anion sites in hydroxylpyromorphite can contain either anion; however, full occupancy of the z=0 position by O defines the end-member

TABLE 3. Comparison of crystallographic data for hydroxylpyromorphite to various synthetic pyromorphites

	Hydroxylpyromorphite (This work)	Pb₅(PO₄)₃OH (Barinova et al. 1998)	Pb₅(PO₄)₃OH (Brückner et al. 1995)	$Pb_{5}(PO_{4})_{3}F$ (Fleet et al. 2010)	Pb₅(PO₄)₃F (Belokoneva et al. 1982)
	, , ,	,		,	,
a (Å)	9.7872(14)	9.774(1)	9.866(3)	9.7638(6)	9.760(8)
c (Å)	7.3070(10)	7.291(1)	7.426(2)	7.2866(4)	7.300(8)
V (ų)	606.2	603.2	625.9	601.6	602.2
Calculated density	7.340	7.356	7.177	7.397	7.389
<pb1-o></pb1-o>	2.703	2.701	2.767	2.696	2.714
<pb2-o f=""></pb2-o>	2.708	2.702	2.703	2.704	2.683
<pb2-pb2></pb2-pb2>	4.314	3.961	4.227	3.953	4.327
Pb2-OH/F	2.932/2.58	2.925	2.896	2.752	2.954
<p1-o></p1-o>	1.544	1.539	1.509	1.533	1.566
Pb1 metaprism twist angle (°) 21.6	22.1	26.7	22.7	23.6

species. Our inability to distinguish O and F by site scattering does not affect our analysis of the anion ordering except for the location of the hydroxyl H atom, which for F at z = 0 and O at z = 0.087 would either occur near z = -0.23 or -0.05. The corresponding donor-acceptor distances for this configuration become very long, >3.6 Å for H at z = 0.23, or very short, ~ 2.4 Å (z = 0.05), and may account for the relatively strong hydrogenbonding interactions ($\sim 2.7 \text{ Å}$) observed in the infrared spectrum. Although no electron density was observed for z > 0.14, diffraction contributions of H atoms to the disorder may not be significant or are obscured in the presence of heavier scattering atoms. Additional synthetic studies are needed to better understand the effects of Cl, F, and OH content on anion-column ordering and hydrogen-bonding in tertiary pyromorphites. Nevertheless, our findings for fluoride-rich hydroxylpyromorphite suggest that solid solution between the yet undescribed mineral "fluorpyromorphite" and hydroxylpyromorphite is possible.

IMPLICATIONS

Consumption of lead-contaminated water can lead to serious health problems, especially in children, and there is currently no tolerable level of lead exposure identified by the Centers for Disease Control and Prevention (2013). In like manner, the Environmental Protection Agency uses a "maximum contaminant level goal" of zero for Pb (U.S. EPA 2019). Rather than an acceptable minimum contaminant level as used for other contaminants, there are treatment regulations in place when "action-level" (0.015 mg/L) lead concentrations are reached. When concentrations above the action level are found, the socalled Lead and Copper Rule is applied, whereby municipal water plants introduce corrosion control by adjusting pH, lowering dissolved carbonate content, and adjusting the Cl⁻/SO₄² ratio with the coagulants ferric chloride or ferric sulfate (U.S. EPA 2019; Nguyen et al. 2011). These treatments reduce the corrosion rate of pipes and leaded solder joints, lowering Pb levels at the tap; however, treatment of the source water itself is at times necessary in aquifers with high levels of Pb or other contaminants. One of the most commonly applied methods for direct removal of Pb is the addition of phosphoric acid. When added to Pb-contaminated water, phosphoric acid will initially cause precipitation of hydroxylpyromorphite due to its significantly lower solubility than hydroxylapatite, $K_{\rm sp} = \sim 10^{-81}$ vs. $\sim 10^{-58}$ (Zhu et al. 2016); and indeed, hydroxylpyromorphite was identified as a corrosion product of lead pipes in laboratory experiments (Grimes et al. 1995) and within the city of Glasgow, Scotland, U.K., municipal water supply (Peters et al. 1999).

In practice, higher concentrations of Ca, Cl, and F in drinking water may lead to precipitation of mixed-anion and dominantly Ca- and Cl-bearing apatite phases that incorporate trace Pb depending on the local chemistry. However, Pb was efficiently immobilized in contaminated soils mixed with finely ground fluorapatite-bearing rocks in experiments by Ma et al. (1995), who observed that the primary mechanism of Pb immobilization was precipitation of a "fluoropyromorphite"-like mineral. Likewise, experiments by Valsami-Jones et al. (1998) and Mavropoulos et al. (2002) reveal that release of Pb from less soluble apatite phases can occur by slow diffusion, with re-uptake into newly precipitated hydroxylpyromorphite layers occurring on

their surfaces.

Our investigations of hydroxylpyromorphite suggest solid solution is possible between it and other apatite-supergroup members, specifically the undescribed minerals "fluorpyromorphite" and "hydroxylphosphohedyphane," but further work is needed to understand how excess chloride may affect the anion-column arrangement and hydrogen bonding for binary (F-Cl, OH-Cl, F-OH) or tertiary (F-Cl-OH) substitutions. The full description of hydroxylpyromorphite presented here may inspire future synthetic studies to provide a deeper understanding of the relationship between anion-column ordering and resultant properties, such as solubility, reactivity, and Pb mobility in complex systems. This information could help optimize remediation and corrosion control for a wider variety of Pb-contaminated aquifers and soils.

ACKNOWLEDGMENTS AND FUNDING

We thank reviewers Uwe Kolitsch and John M. Hughes for valuable comments that improved the quality of this manuscript. Support for this work was provided by the Chemical Sciences, Geosciences and Biosciences Division, Office of Basic Energy Sciences, Office of Science, U.S. Department of Energy, Grant No. DE-FG02-07ER15880. We thank the ND Energy Materials Characterization Facility for use of the single-crystal X-ray diffractometer. A portion of this study was funded by the John Jago Trelawney Endowment to the Mineral Sciences Department of the Natural History Museum of Los Angeles County.

REFERENCES CITED

- Anthony, J.W., Bideaux, R.A., Bladh, K.W., and Nichols, M.C. (2000) Handbook of Mineralogy. Mineral Data Publishing, Tucson, Arizona, U.S.A.
- Armstrong, J.T. (1988) Quantitative analysis of silicates and oxide minerals: Comparison of Monte-Carlo, ZAF and Phi-Rho-Z procedures In D.E. Newbury, Ed., Microbeam analysis. San Francisco Press, Inc.
- Badraoui, B., Aissa, A., Bigi, A., Debbabi, M., and Gazzano, M. (2006) Structural investigations of lead-strontium fluoroapatites. Journal of Solid State Chemistry, 179, 3065–3072
- Baikie, T., Schreyer, M., Wei, F., Herrin, J.S., Ferraris, C., Brink, F., Topolska, J., Piltz, R.O., Price, J., and White, T.J. (2014) The influence of stereochemically active lone-pair electrons on crystal symmetry and twist angles in lead apatite-2H type structures. Mineralogical Magazine, 78, 325–345.
- Barinova, A.V., Bonin, M., Pushcharovskii, D.Y., Rastsvetaeva, R.K., Schenk, K., and Dimitrova, O.V. (1998) Crystal structure of synthetic hydroxylpyromorphite Pb₅(PO₄)₃(OH). Crystallography Reports, 43, 189–192.
- Belokoneva, E.L., Troneva, E.A., Dem'yanets, L.N., Duderov, N.G., and Belov, N.V. (1982) Crystal structure of synthetic fluoropyromorphite Pb₅(PO₄)₃F. Kristallografiya, 27, 793–794 (in Russian).
- Bigi, A., Ripamonti, A., Brückner, S., Gazzano, M., Roveri, N., and Thomas, S.A. (1989) Structure refinements of lead-substituted calcium hydroxyapatite by X-ray powder fitting. Acta Crystallographica, B45, 247–251.
- Brückner, S., Lusvardi, G., Menabue, L., and Saladini, M. (1995) Crystal structure of lead hydroxyapatite from powder X-ray diffraction data. Inorganica Chimica Acta, 236, 209–212.
- Carlson, S.M., Laughlin-Yurs, C., Olds, T.A., Fountain, D.R., and Mills, O.P. (2017) Secondary Lead Minerals from the Copps Mine, Gogebic County, Michigan. Rocks and Minerals, 92, 166–171.
- Centers for Disease Control and Prevention (CDC) (2013) Blood lead levels in children aged 1–5 years – United States 1999–2010. MMWR, Morbidity and Mortality Weekly Reports, 62(13), 245–248.
- Cockbain, A.G. (1968) Lead apatite solid-solution series. Mineralogical Magazine and Journal of the Mineralogical Society, 36, 1171–1173.
- Dai, Y., and Hughes, J. (1989) Crystal-structure refinements of vanadinite and pyromorphite. Canadian Mineralogist, 27, 189–192.
- Dai, Y., Hughes, J.M., and Moore, P.B. (1991) The crystal structures of mimetite and clinomimetite, Pb₃(AsO₄)₃Cl. Canadian Mineralogist, 29, 369–376.
- Fleet, M.E., Liu, X., and Shieh, S.R. (2010) Structural change in lead fluorapatite at high pressure. Physics and Chemistry of Minerals, 37, 1–9.
- Gagné, O.C., and Hawthorne, F.C. (2015) Comprehensive derivation of bond-valence parameters for ion pairs involving oxygen. Acta Crystallographica, B71, 562–578.
- Grimes, S.M., Johnston, S.R., and Batchelder, D.N. (1995) Lead carbonatephosphate system: Solid-dilute solution exchange reactions in aqueous systems. Analyst, 120, 2741–2746.
- Hatert, F., Mills, S.J., Pasero, M., and Williams, P.A. (2013) CNMNC guidelines for the use of suffixes and prefixes in mineral nomenclature, and for the preservation of historical names. European Journal of Mineralogy, 25, 113–115.

- Hey, M.H. (1950) An index of mineral species and varieties arranged chemically, with an alphabetical index of accepted mineral names and synonyms, 608 p. Printed by order of the Trustees of the British Museum, London.
- Hughes, J.M., and Rakovan, J.F. (2015) Structurally Robust, Chemically Diverse: Apatite and Apatite Supergroup Minerals. Elements, 11, 165–170.
- Hughes, J.M., Cameron, M., and Crowley, K.D. (1989) Structural variations in natural F, OH, and Cl apatites. American Mineralogist, 74, 870–876.
- Hughes, J.M., Nekvasil, H., Ustunisik, G., Lindsley, D.H., Coraor, A.E., Vaughn, J., Phillips, B.L., McCubbin, F.M., and Woerner, W.R. (2014) Solid solution in the fluorapatite-chlorapatite binary system: High-precision crystal structure refinements of synthetic F-Cl apatite. American Mineralogist, 99, 369–376.
- Hughes, J.M., Harlov, D., Kelly, S.R., Rakovan, J., and Wilke, M. (2016) Solid solution in the apatite OH-Cl binary system: Compositional dependence of solid-solution mechanisms in calcium phosphate apatites along the Cl-OH binary. American Mineralogist, 101, 1783–1791.
- Hughes, J.M., Harlov, D., and Rakovan, J.F. (2018) Structural variations along the apatite F-OH join. American Mineralogist, 103, 1981–1987.
- Ishikawa, T., Wakamura, M., and Kondo, S. (1989) Surface characterization of calcium hydroxylapatite by Fourier transform infrared spectroscopy. Langmuir, 5, 140–144.
- Kampf, A.R., and Housley, R.M. (2011) Fluorphosphohedyphane, Ca₂Pb₃(PO₄)₃F, the first apatite supergroup mineral with essential Pb and F. American Mineralogist, 96, 423–429.
- Kelly, S.R., Rakovan, J., and Hughes, J.M. (2017) Column anion arrangements in chemically zoned ternary chlorapatite and fluorapatite from Kurokura, Japan. American Mineralogist, 102, 720–727.
- Kim, J.Y., Hunter, B.A., Fenton, R.R., and Kennedy, B.J. (1997) Neutron powder diffraction study of lead hydroxyapatite. Australian Journal of Chemistry, 50, 1061–1065.
- Kirchner, E.C., Mrazek, R., and Wimmer, H. (2007) Neue Mineralfunde von Bergbauhalden Radhausberg Süd (Weißental) Kreuzkogel. Mineralogisches Archiv Salzburg, 12, 251–254 (In German).
- Klasner, J.S., LaBerge, G.L., and Cannon, W.F. (1998) Geologic map of the eastern Gogebic iron range, Gogebic County, Michigan. IMAP 2606 (Online). Available: https://pubs.er.usgs.gov/publication/i2606 (accessed July 18, 2020).
- Kolitsch, U., and Lóránth, C. (2016) Descloizit und das Hydroxyl-Analogon von Pyromorphit vom Talkbergbau Rabenwald bei Anger. Der Steirische Mineralog, 31, 52.
- Krause, L., Herbst-Irmer, R., Sheldrick, G.M., and Stalke, D. (2015) Comparison of silver and molybdenum microfocus X-ray sources for single-crystal structure determination. Journal of Applied Crystallography, 48, 3–10.
- Libowitzky, E. (1999) Correlation of O-H stretching frequencies and O-H···O hydrogen bond lengths in minerals. Monatshefte Für Chemie, 130, 1047–1059.
- Lower, S.K., Maurice, P.A., and Traina, S.J. (1998) Simultaneous dissolution of hydroxylapatite and precipitation of hydroxypyromorphite: Direct evidence of homogeneous nucleation. Geochimica et Cosmochimica Acta, 62, 1773–1780.
- Ma, Q.Y., Logan, T.J., and Traina, S.J. (1995) Lead immobilization from aqueous solutions and contaminated soils using phosphate rocks. Environmental Science and Technology, 29, 1118–1126.
- Mavropoulos, E., Rossi, A.M., Costa, A.M., Perez, C.A.C., Moreira, J.C., and Saldanha, M. (2002) Studies on the mechanisms of lead immobilization by hydroxyapatite. Environmental Science and Technology, 36, 1625–1629.
- Nguyen, C.K., Stone, K.R., and Edwards, M.A. (2011) Chloride-to-sulfate mass

- ratio: Practical studies in galvanic corrosion of lead solder. Journal American Water Works Association, 103, 81–92.
- Pasero, M., Kampf, A.R., Ferraris, C., Pekov, I.V., Rakovan, J., and White, T.J. (2010) Nomenclature of the apatite supergroup minerals. European Journal of Mineralogy, 22, 163–179.
- Peters, N.J., Davidson, C.M., Britton, A., and Robertson, S.J. (1999) The nature of corrosion products in lead pipes used to supply drinking water to the City of Glasgow, Scotland, UK. Fresenius' Journal of Analytical Chemistry, 363, 562–565.
- Shannon, R.D., and Prewitt, C.T. (1969) Effective ionic radii in oxides and fluorides. Acta Crystallographica, B25, 925–946.
- Sheldrick, G.M. (2015a) SHELXT—Integrated space-group and crystal-structure determination. Acta Crystallographica, A71, 3–8.
- ——— (2015b) Crystal structure refinement with SHELXL. Acta Crystallographica, C71, 3–8.
- Stock, M.J., Humphreys, M.C.S., Smith, V.C., Johnson, R.D., Pyle, D.M., and EIMF (2015) New constraints on electron-beam induced halogen migration in apatite. American Mineralogist, 100, 281–293.
- Stormer, J.C., Pierson, M.L., and Tacker, R.C. (1993) Variation of F and Cl X-ray intensity due to anisotropic diffusion in apatite during electron microprobe analysis. American Mineralogist, 78, 641–648.
- Sudarsanan, K., and Young, R.A. (1978) Structural interactions of F, Cl and OH in apatites. Acta Crystallographica Section B, 34, 1401–1407.
- Temple, A.K. (1956) V.—The Leadhills-Wanlockhead lead and zinc deposits. Transactions of the Royal Society of Edinburgh, 63, 85–113.
- U.S. Environmental Protection Agency (U.S. EPA) (2019) Optimized corrosion control treatment evaluation technical recommendations for primacy agencies and public water systems (Online). Available: https://www.epa.gov/sites/production/files/2019-07/documents/occtmarch2016updated.pdf (accessed July 18, 2020). U.S. EPA, Washington, D.C.
- Valsami-Jones, E., Ragnarsdottir, K.V., Putnis, A., Bosbach, D., Kemp, A.J., and Cressey, G. (1998) The dissolution of apatite in the presence of aqueous metal cations at pH 2–7. Chemical Geology, 151, 215–233.
- White, T.J., and ZhiLi, D. (2003) Structural derivation and crystal chemistry of apatites. Acta Crystallographica, B59, 1–16.
- Zhu, Y., Huang, B., Zhu, Z., Liu, H., Huang, Y., Zhao, X., and Liang, M. (2016) Characterization, dissolution and solubility of the hydroxypyromorphite– hydroxyapatite solid solution [(Pb_xCa_{1-x})₅(PO₄)₃OH] at 25 °C and pH 2–9. Geochemical Transactions, 17, 1–18.

Manuscript received March 18, 2020 Manuscript accepted September 5, 2020 Manuscript handled by Aaron Lussier

Endnote:

¹Deposit item AM-21-67516, Online Material. Deposit items are free to all readers and found on the MSA website, via the specific issue's Table of Contents (go to http://www.minsocam.org/MSA/AmMin/TOC/2021/Jun2021_data/Jun2021_data. html). The CIF has been peer reviewed by our Technical Editors.